

# Temperature Estimation Using Ultrasonic Spatial Compound Imaging

Mathieu Pernot, Mickael Tanter, Jeremy Bercoff, Kendall R. Waters, *Member, IEEE*, and Mathias Fink

**Abstract**—The feasibility of temperature estimation during high-intensity focused ultrasound therapy using pulse-echo diagnostic ultrasound data has been demonstrated. This method is based upon the measurement of thermally-induced modifications in backscattered RF echoes due to thermal expansion and local changes in the speed of sound. It has been shown that strong ripple artifacts due to the thermo-acoustic lens effect severely corrupt the temperature estimates behind the heated region. We propose here a new imaging technique that improves the temperature estimation behind the heated region and reduces the variance of the temperature estimates in the entire image. We replaced the conventional beamforming on transmit with multiple steered plane wave insonifications using several subapertures. A two-dimensional temperature map is estimated from axial displacement maps between consecutive RF images of identically steered plane wave insonifications. Temperature estimation is then improved by averaging the two-dimensional maps from the multiple steered plane wave insonifications. Experiments were conducted in a tissue-mimicking gelatin-based phantom and in fresh bovine liver.

## I. INTRODUCTION

THE feasibility of temperature estimation during high-intensity focused ultrasound (HIFU) therapy using pulse-echo diagnostic ultrasound data has been demonstrated by Seip *et al.* [1], [2]. HIFU is a promising therapeutic technique for the treatment of deep localized cancers [3], [4]. However, improved monitoring methods are necessary before HIFU can be clinically useful. Accurate treatments specifically require that temperature elevations in the treatment volume be controlled with appropriate feedback. Over the past decade, several research groups have focused on non-invasive temperature estimation using magnetic resonance imaging [5]–[7] and ultrasonic imaging [2], [8], [9]–[12]. Both of these techniques have their own advantages and limitations. Magnetic resonance imaging of temperature provides quasi-real time three-dimensional temperature maps with a very good localization of the heated region, but is costly to use. In contrast, ultrasound techniques can be easily integrated into HIFU systems with relatively low cost and a high portability.

Seip and Ebbini [2] and Simon *et al.* [8] have recently

proposed a method for two-dimensional (2D) real-time non-invasive temperature estimation using diagnostic ultrasound. This technique is based on tracking the shifts in the backscattered RF signals (i.e., speckle) due to thermal expansion and local changes in the speed of sound. The cumulative time-shifts are differentiated along the axial direction to obtain a one-dimensional temperature map with multiple scan lines used to construct a 2D temperature map. Simon *et al.* [8] have shown that a 2D map of the temperature distribution can be estimated with a very good temperature resolution ( $< 0.5^\circ\text{C}$ ) and a high spatial resolution in a tissue-mimicking phantom and in *ex vivo* tissues. However, we note that currently no *in vivo* experiments have demonstrated the potential of this technique in clinical situations. An important limitation of this technique is the spatial ripple introduced by sharp lateral gradients in the temperature distribution through the thermo-acoustic effect [8], [13]. Because the speed of sound in the heated region is significantly changed, it acts as an aberrator for the diagnostic ultrasound system, and artifacts severely corrupt the temperature change estimates. Simon *et al.* [8] suggested introducing 2D spatial filters to reduce the ripple artifacts. However, it is difficult to discriminate the spatial frequency dependence of the ripples and of the temperature distribution at the focus. Furthermore, spatial filters reduce the artifacts only partially with the added cost of reduced spatial and temperature resolution.

An elegant diagnostic ultrasound imaging technique, known as *ultrasonic spatial compound imaging*, was developed to reduce the “speckle noise” texture of echographic images. This compound imaging approach has been extensively investigated over the two past decades [14], [15], and studies have demonstrated its ability to strongly reduce the variance of the speckle. In addition, this imaging technique has been implemented on a commercial ultrasound scanner (i.e., Philips ATL HDI 5000), where it has been shown to enhance image quality by reducing acoustic artifacts [16]. Recently, Tanter *et al.* [17] applied this technique to 2D motion vector estimation in the field of ultrasound-based elastography. In particular, they have demonstrated that the variance of displacement estimates can be significantly reduced by the use of compounded plane or weakly focused wave insonifications.

In this paper we apply the spatial-compounding technique for 2D temperature estimation and reduction of the thermal lens effect. In Section II, the compound-imaging system and the basic principles of acquisition sequences are presented. In Section III, experiments are performed on

Manuscript received October 3, 2003; accepted December 19, 2003. M. Pernot, M. Tanter, J. Bercoff, and M. Fink are with the Laboratoire Ondes et Acoustique, ESPCI, Université Paris VII, U.M.R. C.N.R.S. 7587, 10 rue Vauquelin, 75005 Paris, France (e-mail: mathieu.pernot@loa.espci.fr).

K. R. Waters is with NIST, 325 Broadway, Boulder, Colorado 80305.

tissue-mimicking (TM) phantoms and fresh bovine liver. The optimization of the compounding sequences is discussed, including the number of steered plane waves and the size of transmit subapertures. In addition, the strong decorrelation effects due to tissue necrosis are investigated. In Section IV, the limitations of this technique are discussed, and improvements are proposed.

## II. MATERIAL AND METHODS

### A. Two-Dimensional Temperature Estimation

Ultrasonic estimation of temperature is based upon the thermal dependence of the RF pulse-echo signals, as discussed by Seip *et al.* [2]. Two physical phenomena are involved in the modification of the speckle during heating: the temperature dependence of the speed of sound and the thermal expansion of the tissue. Because standard receiver beamforming algorithms assume a constant speed of sound, apparent displacements of the ultrasonic scatterers in the B-scan image are produced. In addition, the thermal expansion introduces physical displacements of the scatterers. Both apparent and physical displacements are accumulated along the ultrasound beam axis. The change in temperature  $\Delta T(z)$  along the beam axis can then be related to the axial displacements according to [8]:

$$\Delta T(z) = \frac{c_0}{2(\alpha - \beta)} \frac{\partial t(z)}{\partial z}, \quad (1)$$

where  $t(z)$  is the estimated time-shift at depth  $z$ ,  $c_0$  is the initial speed of sound in the medium,  $\alpha$  is the linear coefficient of thermal expansion, and the coefficient  $\beta = 1/c_0 \cdot \partial c / \partial T$  relates the change in the speed of sound with temperature. In this model it is assumed that the variation of speed of sound with respect to temperature is linear over a limited range of temperature elevation, typically up to 45°C. The coefficient  $k = 1/(\alpha - \beta)$  is a constant parameter that can be experimentally determined. It depends on tissue type and fat content [12], [18]. Indeed the temperature-dependence coefficient of sound speed  $\beta$  is positive for mammalian tissues, except for fat, which has a strong negative coefficient.

The time-shift occurring between two successive RF images is estimated using a classical speckle tracking technique: one-dimensional cross-correlations performed along the ultrasound beam axis. Small overlapping data windows of  $8\lambda$  (where  $\lambda$  is the wavelength) are used in this algorithm. This method is simple to implement, is computationally efficient, and provides an accurate estimation of small time-shifts ( $\sim 10$  ns). Once the 2D time-shift map is estimated, the temperature map is computed by differentiating the time-shift estimates along the axial direction.

Simon *et al.* [8] have demonstrated that this technique provides accurate real-time temperature estimation in a heated region of a rubber phantom. Behind this region, however, the temperature estimation is severely corrupted by ripple artifacts. The receiver beamforming does not

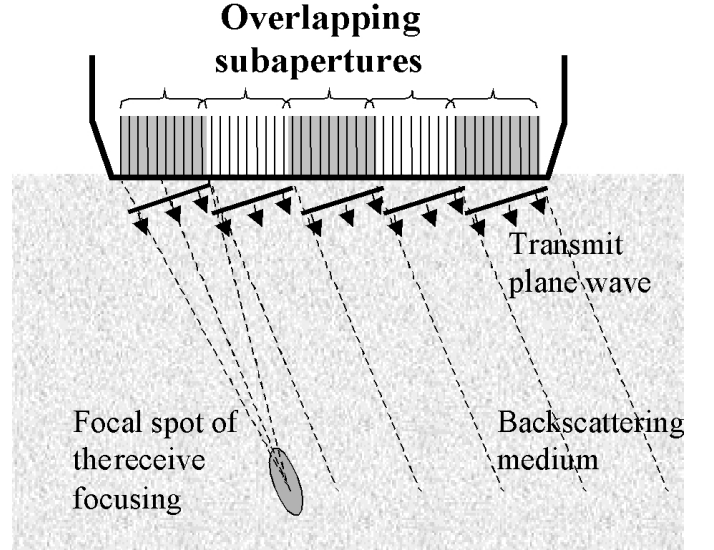


Fig. 1. Compound imaging sequence. Transmit mode: a plane wave is electronically steered using transmit subapertures. Receive mode: the backscattered signals are beamformed with the receive focus steered in the same direction.

compensate for the inhomogeneous distribution of the speed of sound. Consequently, large lateral gradients in temperature induce decorrelation in the time-shift estimation behind the heated region.

### B. Compound Imaging

Because of the strong thermo-acoustic lens effect, the diagnostic imaging system cannot “see” accurately behind the heated region. We propose using multiple viewing angles to reduce this acoustic lens effect. Here, we briefly discuss how compound imaging is implemented for 2D temperature estimation and the corresponding modifications to the conventional imaging technique that are necessary.

The medium is insonified successively with several ultrasonic plane waves steered with different angles, instead of using a conventional beamforming on transmit. Each plane wave is transmitted by limited overlapping subapertures, as shown in Fig. 1, in order to reduce the size of the region that can contribute to the received ultrasonic echo. Sixty-four elements (of 128 elements total) are used in the receive beamforming algorithm, and the receive focal spot is steered with the same angle as the transmit plane wave. Thus, there is focusing only on reception. This choice was made due to current memory limitations of our laboratory imaging system (see Section III-A). However, using real-time compounding with both transmit and receive focusing is also conceivable for temperature estimation.

Fig. 2 shows the steps involved in the heating and imaging sequences. Data acquisition occurs in real time. All backscattered echoes are stored in the system memory during heating, and beamforming on reception is performed off-line. Ultrasonic images are constructed for each steering angle before and after heating. The time-shifts are then estimated between speckle images corresponding to iden-

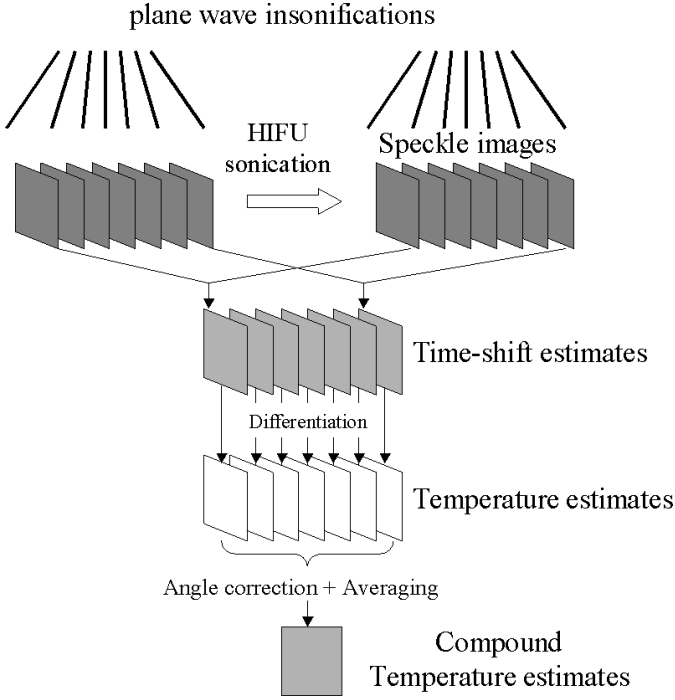


Fig. 2. Temperature estimation with compound imaging. The medium is insonified by multiple steered plane waves and the corresponding RF data are collected. The two sets of RF-beamformed data (before and after heating) are cross-correlated and a time-shift map is determined. The time-shift estimates are differentiated along the axial direction (i.e., the beam-steering axis) to estimate temperature. The temperature estimates for the multiple steered plane waves are then averaged with angle correction and correlation value weighting.

tical plane wave insonifications. Each time-shift map is spatially differentiated along its axial direction in order to estimate the change in temperature. Because the axial direction of each steered plane wave insonification is different, the individual temperature maps are numerically steered back to the same direction. For a given steering angle  $\vartheta_n$  and a location  $(x, z)$ , the temperature  $T_n(x, z)$  and a corresponding correlation value  $c_n(x, z)$  are estimated. The correlation coefficient gives an index of confidence for the cross-correlation performance, and permits determination of a weighted average of the temperature. The compounded temperature estimate  $\langle T(x, z) \rangle$  for  $N$  steering angles is then:

$$\langle T(z, z) \rangle = \frac{1}{\sum_{n=1}^N c_n(x, z)} \sum_{n=1}^N c_n(x, z) T_n(x, z) \quad (2)$$

### C. Experimental Setup

The HIFU transducer was composed of a 56-element piezocomposite spherical annular array (14 rings, quartered). The transducer had a diameter of 100 mm, a focal length of 70 mm, and center frequency of 1.5 MHz. The focal zone dimensions of the HIFU transducer were measured at low acoustic intensity ( $< 5 \text{ W cm}^{-2}$ ) in a tank filled with

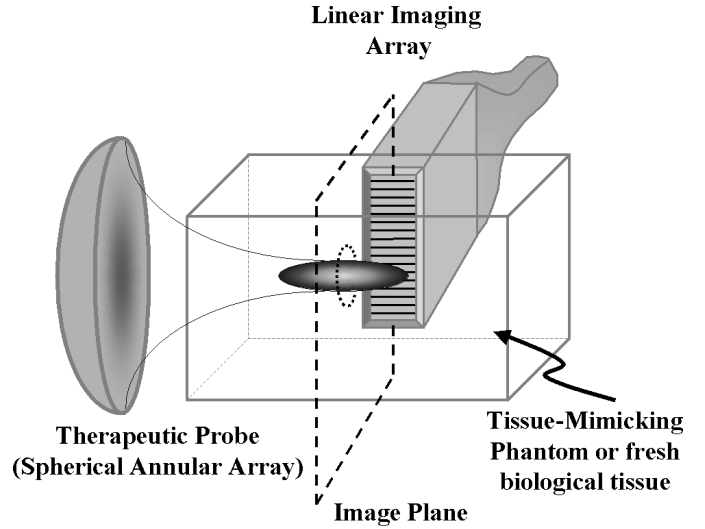


Fig. 3. Experimental setup of the therapy and monitoring system.

degassed water. A 0.4 mm PVDF bilaminar calibrated hydrophone (Golden Lipstick model, SEA, Soquel, CA) was moved using a stepper-motor-controlled three-dimensional positioning system (Micro-controlle). The  $-6 \text{ dB}$  focal zone was  $(1.2 \times 1.2 \times 7.5) \text{ mm}^3$ . Each element was connected to a high power electronic emission board with adjustable amplitude and phase which could deliver up to 16 W.

The imaging probe was a commercial linear imaging array working at 5 MHz (Model L4-7, Philips ATL, Bothel, WA). The field of view was 38 mm (lateral) by 60 mm (axial). The imaging array was mounted on a manually driven Cartesian manipulator and oriented perpendicular to the HIFU beam axis such that it imaged a cross-section of the HIFU focal zone (see Fig. 3). In Section III we discuss an alternative geometry for use under *in vivo* conditions.

The compound imaging acquisitions were performed using a fully programmable multichannel system (128 independent channels) developed in our laboratory. Each channel has an electronic transmitter/receiver board with 2 MB memory. The sequences of steered plane waves using transmitting subapertures can be stored in static RAM. A computer was used to control and trigger the operation of the HIFU electronic system and the imaging system. To avoid interferences between the HIFU and imaging systems, the imaging data were acquired during a 20-ms interruption of the HIFU beam. Thus, heating and imaging sequences could be programmed for real-time acquisitions, as depicted in Fig. 4.

In addition to the fully programmable imaging system, a commercial ultrasound scanner (HDI 1000, Philips ATL, Bothel, WA) was used to provide reference images of temperature using a conventional (i.e., no compounding) imaging technique with a linear array (Model L7-4, Philips ATL, Bothel, WA). Conventional RF-beamformed data were stored during heating and then processed off-line. This permits comparison of conventional and compound imaging techniques for temperature estimation using the same experimental configuration.

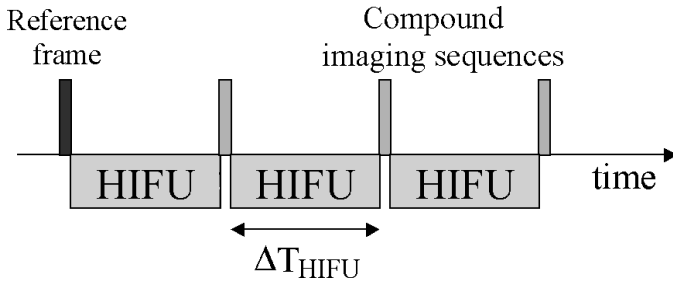


Fig. 4. Real-time therapy and monitoring acquisition sequences.

#### D. Tissue Mimicking Phantom

The TM phantom was composed of 8% gelatin solution with 2% agar powder acting as ultrasonic scatterers. Thermal and acoustical properties of the TM phantom were very similar to those of soft tissues. The speed of sound was measured to be  $1550 \text{ m s}^{-1}$  at  $25^\circ\text{C}$ . The material-dependent parameter  $k$  was determined experimentally to be  $(-980 \pm 40)^\circ\text{C}$ . To determine  $k$ , the phantom and the imaging probe were placed in a temperature-controlled water bath, and RF data were acquired while the water was heated from  $19$  to  $40^\circ\text{C}$ . The time-shifts between two successive acquisitions were estimated. The constant  $k$  was determined by differentiating the time-shifts in the axial direction, and then fitting the water bath temperature to (1). A reference temperature was measured by a coated copper-constantan thermocouple sensor (wire size:  $75 \mu\text{m}$ , junction size:  $< 0.22 \text{ mm}$ , type IT-23, Physitemp Instruments, Inc., Clifton, NJ) placed in the phantom.

### III. EXPERIMENTS AND RESULTS

#### A. Evaluation of Compound Imaging Technique

Experiments were initially performed on TM phantoms to evaluate the ability of the compound imaging technique to improve temperature estimation. We compared ultrasonic estimates of temperature using the compounding technique with thermocouple measurements. We considered how the number of steered angles and subapertures affected the variance in the temperature maps. Finally, we compared temperature estimates using compounding and conventional imaging techniques.

1. *Thermocouple Measurements:* Compound imaging measurements were performed on a TM phantom with an implanted thermocouple sensor. The phantom was placed such that the thermocouple sensor was located in the focal plane of the HIFU probe, 2 mm away from the focus. In this configuration the sensor and the ultrasonic beam were far enough apart to avoid thermocouple artifacts [19]. A reference imaging sequence was composed of 5 steered plane waves on transmit (steering angles  $-10^\circ$ ,  $5^\circ$ ,  $0^\circ$ ,  $5^\circ$ , and  $10^\circ$ ). Each transmit subaperture was composed of 30 elements (corresponding to 10-mm width), and the receive

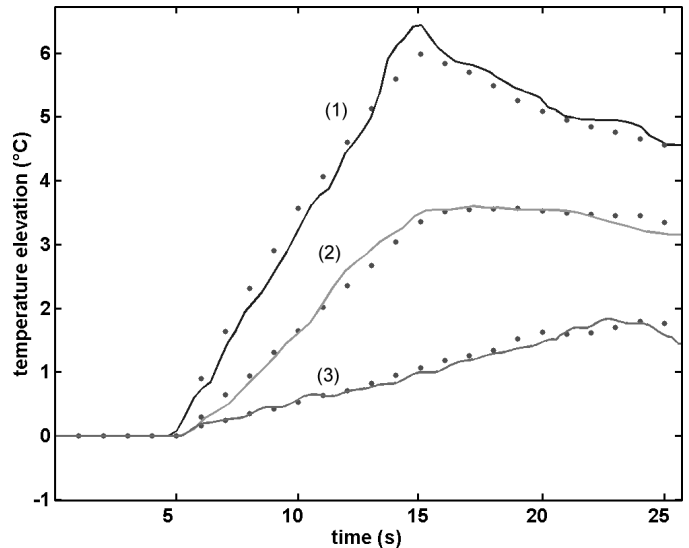


Fig. 5. Temperature measured by thermocouple (line) and estimated by ultrasound (dot) at (1) 2 mm; (2) 3 mm; and (3) 4 mm from focus.

subaperture was made of 64 elements. The therapeutic field ( $150 \text{ W cm}^{-2}$  at focus) was applied during 10 s, and then the phantom was allowed to cool down. Every second the therapeutic beam was interrupted for 20 ms and a compound imaging sequence was performed. Available memory of the imaging electronics permitted storage of 20 monitoring sequences (e.g., 20 frames at 1 frame/s). The RF data were collected and beamformed, and the compounded temperature maps were computed. The experiment was repeated for other locations of the thermocouple sensor: the phantom was moved such that the HIFU focus was located 3 mm and 4 mm away from the thermocouple sensor. Fig. 5 shows that there was good agreement between the thermocouple measurements and the ultrasonic estimates of temperature at different sensor locations. The average error in non-invasive temperature estimation was  $0.14^\circ\text{C}$  for a total temperature elevation of  $12.3^\circ\text{C}$  at the focus.

2. *Optimization of Compound Imaging Technique:* We investigated the dependence of the artifact reduction as a function of the number of transmit plane waves and the size of the subapertures. The optimal number of transmit plane waves is a compromise between the image frame rate and the reduction in variance of the temperature estimates. We note that this optimization also depends upon the geometry of the experiment. A complete temperature estimation experiment was performed with an imaging sequence of 29 transmit plane waves. The steering angles of the plane waves ranged from  $-14^\circ$  to  $14^\circ$  with a step of  $1^\circ$ . Heating was applied for 5 s using an HIFU field of  $130 \text{ W cm}^{-2}$  acoustic intensity at the focus. A second RF-beamformed data set was acquired immediately after heating. A set of 15 different temperature maps was processed by taking into account a varying number of transmit plane waves (i.e., 1, 3, 5, ..., 29). The variance of the tempera-

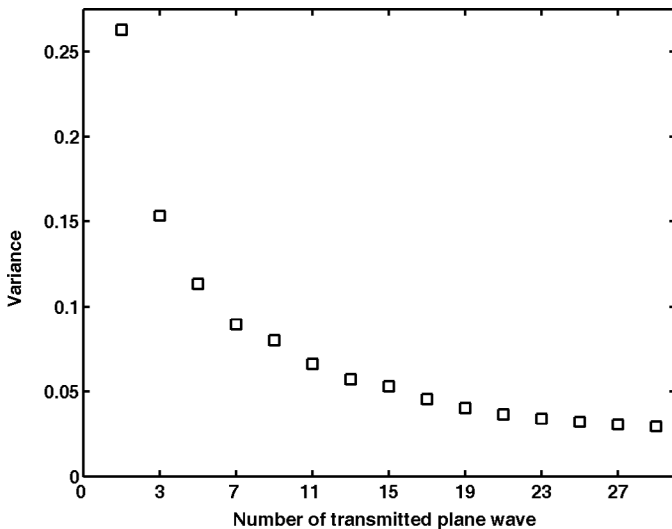


Fig. 6. Variance of the artifacts in the temperature estimation as a function of the number of steered plane waves. The variance is computed over a  $(15 \times 15)$ -mm<sup>2</sup> region located behind the heated region. The plane waves are steered with angles from  $-14^\circ$  to  $14^\circ$  with various step sizes.

ture estimates was calculated in a  $(15 \times 15)$ -mm<sup>2</sup> region immediately behind the focal spot of the HIFU beam in the monitoring image. The temperature elevation at focus was estimated to be  $8^\circ\text{C}$ . As shown in Fig. 6, the variance decreased rapidly with the number of transmitted plane waves. Because this region should have a relatively uniform temperature distribution, a low variance represents a good estimation of the temperature elevation. With seven steered plane wave insonifications, the variance of the artifacts is reduced by more than a factor two. Compound imaging can reduce the speckle variance by as much as a factor of the square root of the number of steered frames. However, for temperature estimation, there remains some correlation in the speckle displacement between the steered frames due to the large spatial extent of the thermo-acoustic lens.

We also investigated the influence of the size of the transmitting subaperture on the reduction in variance. For all imaging sequences, the receive subaperture consisted of 64 elements. The temperature was estimated for seven different imaging sequences where the emission subaperture ranged from 16 to 128 elements. Using all elements on transmit is not optimal because it increases the influence of speckle noise coming from undesired areas. Using too few elements reduces the sensitivity of the transmitted beam and degrades the signal-to-noise ratio in the compounded images. An aperture size corresponding to approximately 30 elements was found to optimize sensitivity as well as speckle motion estimation (see Fig. 7).

*3. Comparison of Compound and Conventional Imaging Techniques:* Compound imaging sequences were composed of 15 steered plane waves on transmit (steering angles from  $-14^\circ$  to  $14^\circ$  with a  $2^\circ$  step) with transmit subapertures of 30 elements. A reference compound imaging sequence was

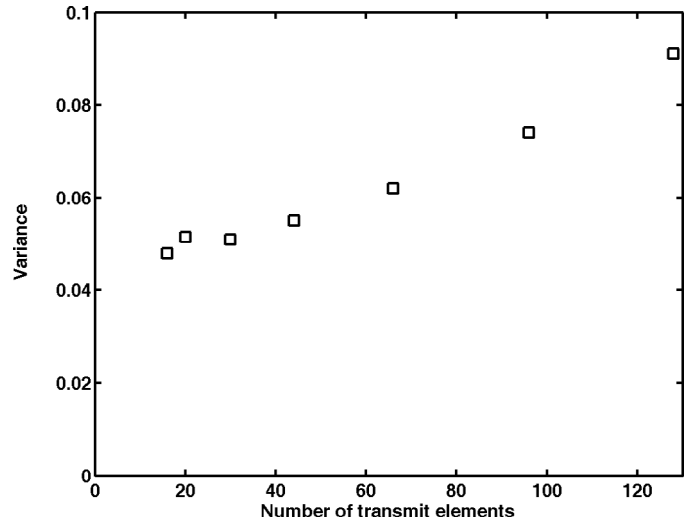


Fig. 7. Variance of the artifacts in the temperature estimation as a function of the number of transmit elements in a subaperture.

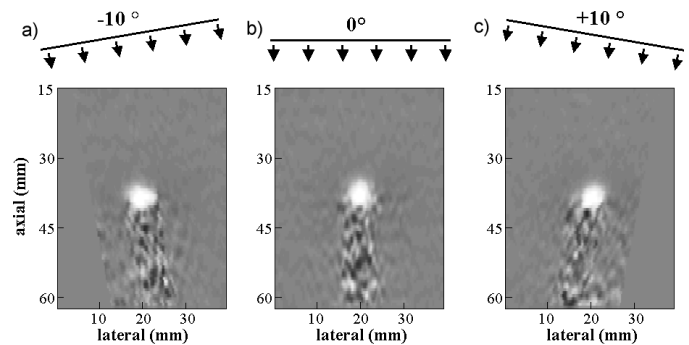


Fig. 8. Two-dimensional temperature estimation for 3 plane-wave insonifications. Steering angles of a)  $-10^\circ$ , b)  $0^\circ$  and c)  $10^\circ$ . The artifacts are aligned with the steering angle.

transmitted and received prior to heating. Heating was applied for 5 s using an HIFU field of  $130 \text{ W cm}^{-2}$  acoustic intensity at the focus. A second RF-beamformed data set was acquired immediately after heating. The RF data were collected and beamformed, and 15 temperature maps (corresponding to the 15 steered plane waves) were computed. We show three of these temperature maps in Fig. 8, with steering angles of  $-10^\circ$ ,  $0^\circ$ , and  $10^\circ$ . One can see clearly that the region of artifact is aligned with the steering angle. Thus, for a given location, the artifacts are strongly decorrelated between images of different steering angles. The compounded 2D temperature estimation was then reconstructed according to (2) and is shown in Fig. 9(a). The B-mode images and the corresponding temperature images have a lateral width of 40 mm and an axial depth of 45 mm. The heating area is located at a 40 mm depth with respect to the imaging probe.

Two-dimensional temperature estimations were also performed with the commercial scanner using conventional B-mode imaging. Prior to heating, a reference RF-beamformed data set was acquired and stored in memory. A second RF-beamformed data set was acquired immedi-

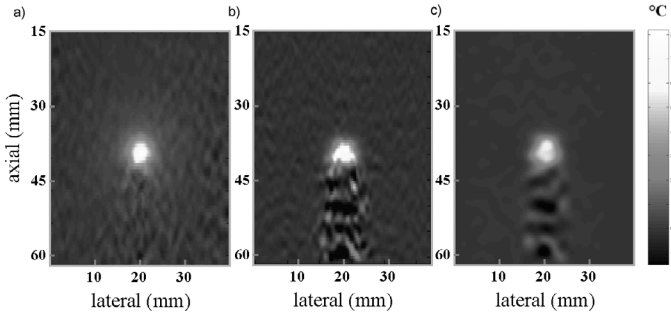


Fig. 9. Two-dimensional temperature estimation by a) compound imaging with our fully programmable electronic device, b) conventional technique with a Philips ATL HDI 1000 scanner, and c) conventional technique with 2D low-pass filtering. The linear imaging transducer was located on the top of the temperature images. The HIFU beam cut perpendicularly the center of the images.

ately after heating. Temperature estimates were then computed as described in Section II-A. The 2D temperature estimation is shown in Fig. 9(b). The temperature is well estimated in the heating zone, but ripple artifacts severely corrupt the region behind the heated area. Artifacts (up to  $7^{\circ}\text{C}$ ) can be almost as large as the temperature elevation at the focus ( $8.2^{\circ}\text{C}$ ). In order to reduce these artifacts, a spatial low-pass filtering was applied along axial and lateral directions, as proposed in [8]. The time-shift estimates were filtered using an axial differentiator and smoothing filter, with the parameters given in [8] (axial filter: 6 dB bandwidth  $0.22\text{ mm}^{-1}$ , length 12.3 mm; lateral filter: 6 dB bandwidth  $0.21\text{ mm}^{-1}$ , length 6.2 mm). Fig. 9(c) shows the filtered temperature estimates. 2D filtering reduced the artifacts in temperature estimation (up to  $1.8^{\circ}\text{C}$ ) but also introduced a bias in the estimate of the peak temperature (temperature elevation at the focus was found to be  $6.3^{\circ}\text{C}$ ).

It is evident that compound imaging strongly reduces the artifacts in temperature estimation. Here, artifacts were almost completely removed when averaging the 15 frames. Moreover, the heated region was very well reconstructed, symmetrical, and the temperature at focus identical to the one estimated in the classical temperature estimation [Fig. 9(b)]. Ultrasonic estimation of the temperature elevation at the HIFU focus was also corroborated by thermocouple measurements as described above.

*4. Clinical Therapy and Monitoring System:* The present experimental setup (see Fig. 3) was chosen to demonstrate the feasibility of the technique. For practical use of this technique, the therapy and monitoring systems should be coaxial. One concern, however, is that sharp temperature gradients in the elevation direction of the imaging transducer may corrupt the temperature estimates. To gain a measure of this effect, we positioned our linear imaging array along the axial direction of the HIFU probe. Estimation of the change in temperature was performed with compound imaging (30-element transmit subapertures, 11 plane waves with steering angles from  $-10^{\circ}$  to  $10^{\circ}$  with  $2^{\circ}$  step). Heating was applied for 5 s us-

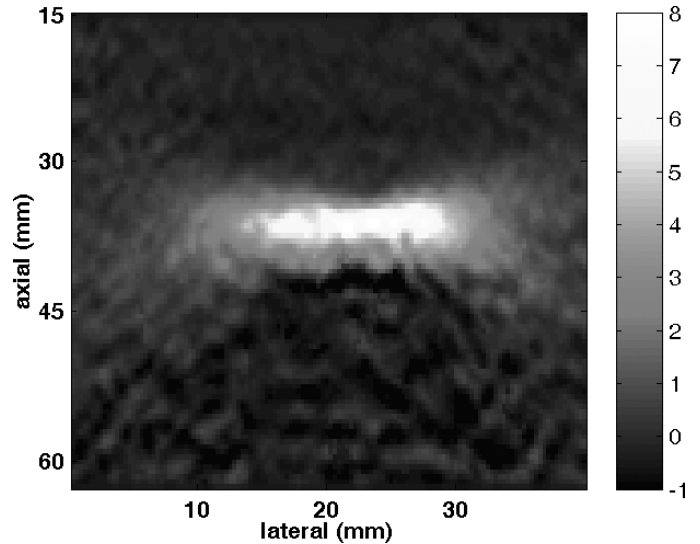


Fig. 10. Temperature change estimation along the axial direction of the HIFU probe. Compound imaging was performed with 30-element transmit subapertures and 11 plane waves with steering angles from  $-10^{\circ}$  to  $10^{\circ}$  with  $2^{\circ}$  step.

ing an HIFU field with  $130\text{ W cm}^{-2}$  acoustic intensity at the focus. A second RF-beamformed data set was acquired immediately after heating. The compounded temperature map is displayed in Fig. 10. As expected in this configuration, the heating zone is cigar-shaped. The heating zone is approximately 10 mm long and 3 mm wide. Moreover, very small artifacts ( $< 1^{\circ}\text{C}$ ) are found behind the focal zone.

## B. In Vitro Bovine Liver Experiments

### 1. Comparison of Compound and Conventional Imaging Techniques:

The compound imaging technique for temperature estimation was validated in fresh bovine liver specimens. The objective was to demonstrate that this technique performed well in soft biological tissues, and could be used for guidance and monitoring of HIFU therapies. The same experimental setup (see Fig. 3) used for the TM phantoms was used for these experiments. Measurements were performed in fresh degassed bovine liver. The initial temperature was  $33^{\circ}\text{C}$ .

Prior to heating, a compound imaging sequence was performed with 30-element transmit subapertures and 11 steered plane waves (steering angles of  $-10^{\circ}$  to  $10^{\circ}$  with  $2^{\circ}$  step). A  $400\text{ W cm}^{-2}$  HIFU sonication was applied for 5 s. Compound imaging sequences were transmitted and received at 1 s, 3 s, and 5 s. The RF data were collected and beamformed, and the temperature was then estimated. The material-dependent parameter  $k$  was set to  $-1200^{\circ}\text{C}$ , based on several studies in liver tissues [12], [20]. We note that precise measurement of the parameter  $k$  would be necessary for accurate monitoring during therapy.

We compare temperature maps from conventional [Fig. 11(a)–(c)], 2D low-pass filtered [Fig. 11(d)–(f)], and

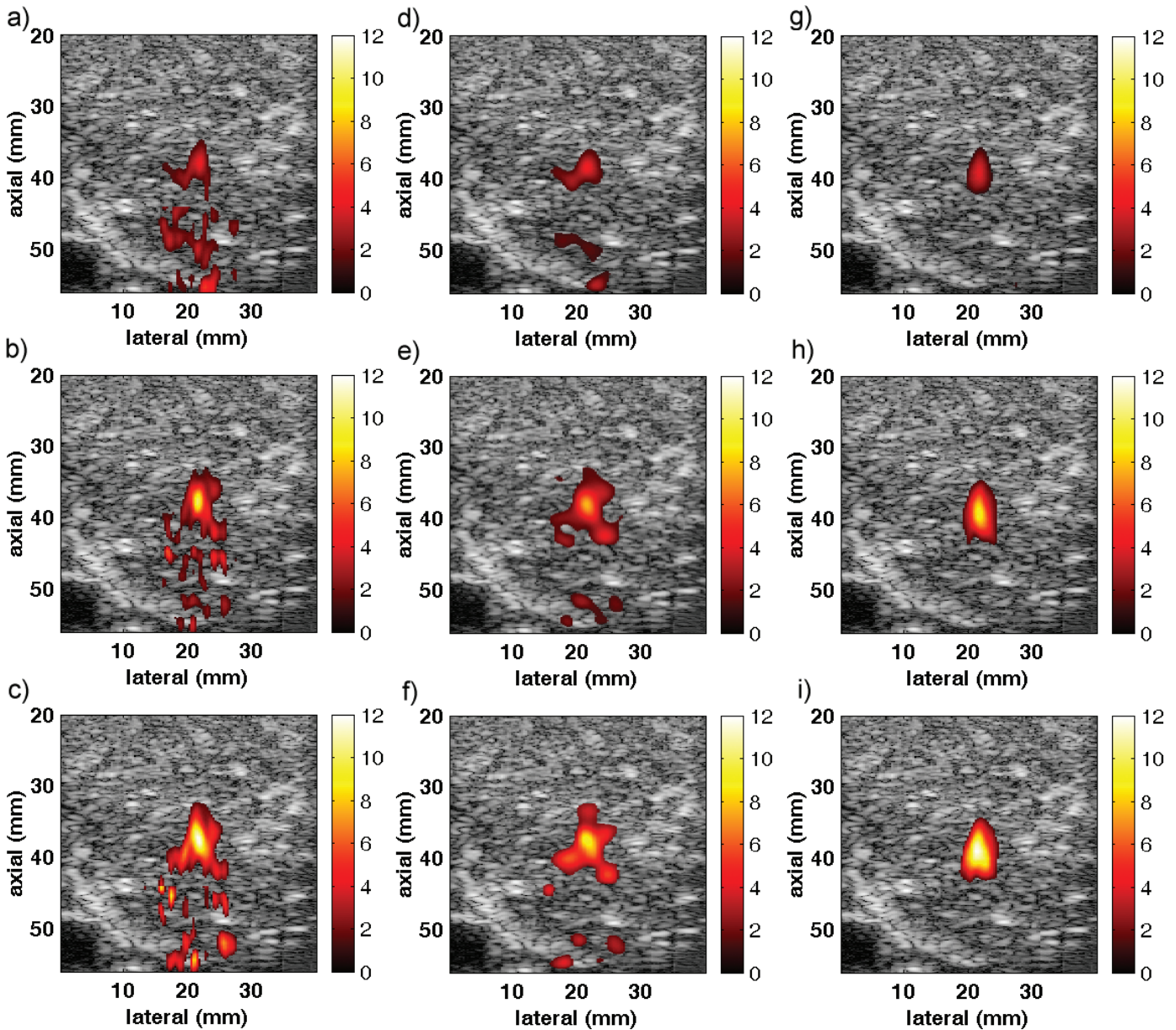


Fig. 11. In-vitro experiment in bovine fresh liver: comparison of compound and conventional imaging techniques. Temperature changes above  $1^{\circ}\text{C}$  overlay the grayscale B-scan image. A sonication was performed with intensity at focus of  $400\text{ W}\cdot\text{cm}^{-2}$ . The temperature changes were estimated following sonication of 1 s (a,d,g), 3 s (b,e,h), and 5 s (c,f,i) for conventional imaging, conventional imaging with 2D low-pass filtering, and compound imaging from left to right, respectively. Compound imaging (g,h,i) was performed using 30-element transmit subapertures and 11 steered plane waves (steering angles of  $-10^{\circ}$  to  $10^{\circ}$  with a step of  $2^{\circ}$ ).

compound [Fig. 11(g)–(i)] imaging techniques. The 2D filter parameters are discussed in Section II-1. Temperature elevations above  $1^{\circ}\text{C}$  are overlaid on the grayscale B-scan image. The temperature elevation of the heated spot was estimated to be  $12^{\circ}\text{C}$  after 5-s sonication. Artifacts are clearly present in the temperature images using the conventional imaging technique. The 2D low-pass filtering reduced artifacts to some extent, but the peak temperature is underestimated. In contrast, compound imaging permits a complete reduction of the artifacts (all artifacts in the images were less than  $1^{\circ}\text{C}$ ) and a good estimation of the peak temperature. This technique was found to have the best performances for guidance and monitoring of HIFU therapies.

2. *Effects of Tissue Necrosis:* For higher temperature elevations, the necrosis threshold was reached and the speckle tracking technique failed to correlate RF data acquired before and after heating. We investigated this decorrelation effect in measurements of bovine liver. HIFU sonications combined with temperature estimation were performed in fresh degassed bovine liver specimens at increasing power levels. The intensity at the focus was increased from  $50\text{ W cm}^{-2}$  to  $800\text{ W cm}^{-2}$ . In each experiment, a compound imaging sequence (30-element transmit subapertures, steering angles from  $-10^{\circ}$  to  $10^{\circ}$  in  $2^{\circ}$  steps) was performed. Following a 5-s HIFU sonication, a post-heating imaging sequence was acquired, and the temperature map was constructed. Lateral slices of the 2D

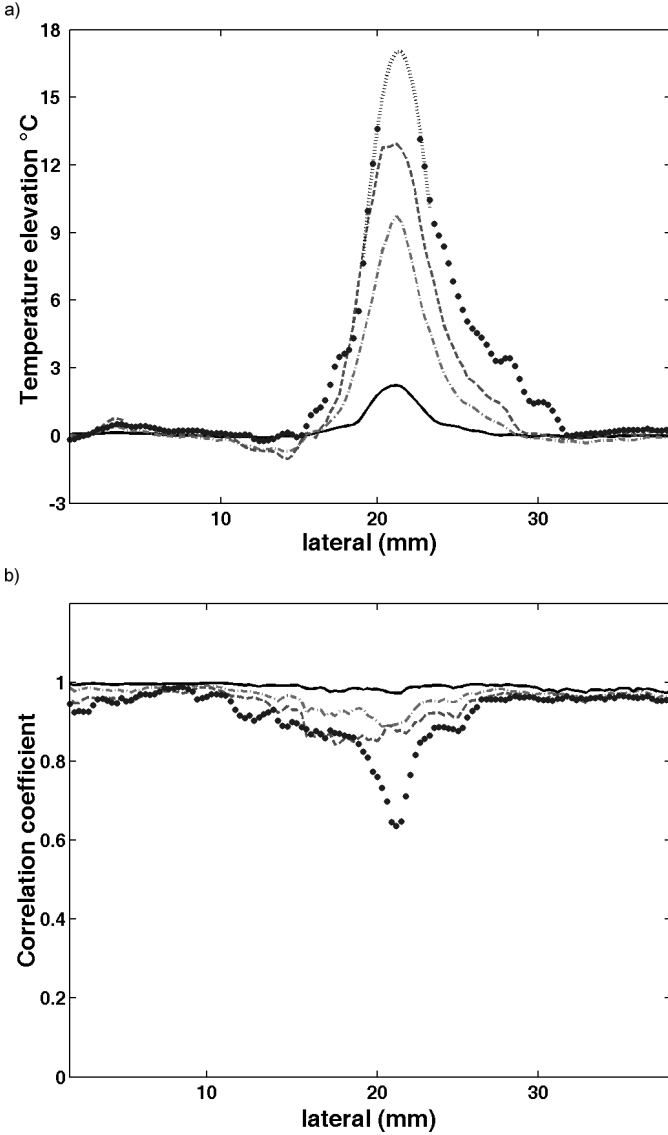


Fig. 12. Lateral slices at the focus of two-dimensional a) temperature distributions and b) correlation coefficients. Experiments were performed in fresh bovine liver at initial temperature of 33°C. The HIFU intensity applied at focus was (-) 50 W cm<sup>-2</sup>, (-.) 200 W cm<sup>-2</sup>, (- -) 450 W cm<sup>-2</sup>, and (\*) 800 W cm<sup>-2</sup> during 5 s. Only temperature change estimates corresponding to correlation coefficients above a 0.80 threshold are displayed. For the 800 W cm<sup>-2</sup> experiment, a Gaussian extrapolation at focus of the temperature change estimates is plotted in black dots.

temperature distribution through the focal plane are plotted in Fig. 12(a) and the corresponding correlation coefficients are shown in Fig. 12(b). The correlation coefficient at the focus for intensities of 50 W cm<sup>-2</sup>, 200 W cm<sup>-2</sup>, and 450 W cm<sup>-2</sup> remained above 0.80, and permitted accurate estimates of temperature. However, at 800 W cm<sup>-2</sup>, the correlation fell below 0.65 in the focal zone, indicating that the temperature was poorly estimated at the focus. In this region, the backscattered signals were significantly altered, and correlation with the initial RF data (i.e., before heating) is degraded. The corresponding temperature map in Fig. 12(a) does not provide a reliable estimate in the heating focal area.

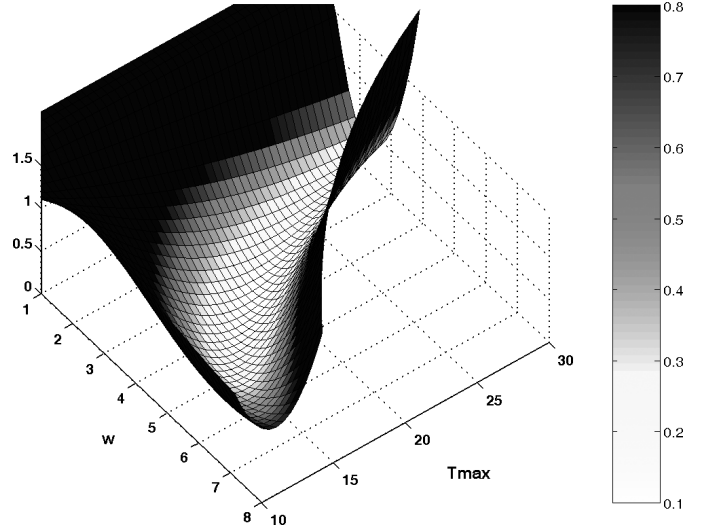


Fig. 13. Least square error of the Gaussian fitting as a function of the curve fitting parameters ( $T_{\max}$ ,  $w$ ). A global minimum of 0.097 was found for  $T_{\max} = 17.6^\circ\text{C}$  and  $w = 3.8$ .

It should be noted, however, that the correlation coefficient is found to be above 0.80 in the major part of the temperature map. Consequently, the temperature at the focus could potentially be extrapolated from these data. The temperature at focus was extrapolated by using a Gaussian fit of the temperature distribution surrounding the focus. Only experimental data with high cross-correlation coefficients ( $> 0.80$ ) were considered relevant. A least square fit was performed using the Gaussian function

$$T(x) = T_{\max} \exp\left(-\left(\frac{x - x_0}{w}\right)^2\right), \quad (3)$$

where  $T_{\max}$  is the temperature at the focus, and  $w$  is the variance of the Gaussian function related to the diffusion coefficient. Fitting of the temperature distributions of the 50 W cm<sup>-2</sup>, 200 W cm<sup>-2</sup>, and 450 W cm<sup>-2</sup> experiments permitted determination of the focus location  $x_0$  and an estimation of the variance ( $w = 3.75$ ). Fig. 13 shows the least squares error between the experimental temperature curve and a Gaussian fit as a function of variance and maximal temperature values ranging from +10°C to +30°C. This error reaches a clear global minimum for  $T_{\max} = 17.6^\circ\text{C}$ . Indeed, this extrapolation corresponds to a robust prediction since the variance ( $w = 3.8$ ) is found to be very similar to the variance found in lower intensity experiments. Thus, estimating the temperature increase in surrounding tissues by assuming a Gaussian diffusion profile of the heat pattern could provide a good prediction of the temperature at focus.

#### IV. DISCUSSION

We have shown in this paper that compound imaging significantly reduces the amount of artifacts in temperature estimates when compared to conventional imaging

techniques. Furthermore, compound imaging can be implemented in real time to provide guidance and feedback of HIFU therapy. Nevertheless, prior to use in a clinical setting, several technical issues must be addressed.

The speckle tracking technique for temperature estimation used here assumes that the thermal dependence of the ultrasonic time-of-flight is linear for small temperature elevations (approximately up to 10°C), which has been verified for biological soft tissues [1], [11]. For higher temperature elevations but below the necrosis threshold, it has been reported [11] that the relation between the ultrasonic time-of-flight and the change in temperature is nonlinear. To compensate for this effect, it has been proposed in [8] to substitute the linear relation in (1) with a nonlinear relation. However, for temperature elevations much higher than 50°C, the major limitation of this temperature estimation technique comes from the irreversible changes in the acoustic properties of tissue due to necrosis. In the case of coagulative necrosis, the acoustical properties of the tissue are completely altered in the heated region with corresponding changes in the backscattered signals. In such a case, the speckle tracking technique fails to correlate RF data acquired before and after heating, and the temperature map is corrupted in the region of necrosis. This effect could be strongly reduced by increasing the imaging frame rate and cross-correlating RF images acquired at a very short time period. However, decorrelation effects can occur even at a high frame rate, and we have shown that estimating the temperature increase in surrounding tissues could provide a robust prediction of the temperature at the focus.

The present experimental setup (see Fig. 3) was chosen to demonstrate the feasibility of the technique. For clinical use of the temperature imaging technique, the therapy and monitoring systems should be coaxial. We are currently developing such a system by placing a linear array within a new HIFU spherical multichannel array. This will provide a more flexible and compact therapy and monitoring probe. In this configuration, sharp temperature gradients will appear in the elevation direction of the imaging transducer, but we have shown that it does not corrupt the temperature estimates.

Another potentially troublesome issue that arises in clinical settings is patient motion, such as respiration. Such motion can lead to strong decorrelation effects. A compensation algorithm for these artifacts has been proposed by Simon *et al.* [21], and has been successfully applied in phantom experiments. Such motion compensation techniques must be improved for practical *in vivo* use, and could then be coupled with the compound imaging method.

In conclusion, the use of spatially compounded plane waves with transmitting subapertures provides significant improvement in the accuracy of the temperature estimation compared to conventional imaging. In particular, the ripple artifacts due to the thermo-acoustic lens effect are greatly reduced. The reduction of these ripple artifacts is a major issue for the promising concept of mixed ultrasonic

therapy/imaging probes. Indeed, for such probes, an imaging array is embedded in the therapy probe vicinity and the imaging plane is parallel to the therapy beam, resulting in particularly strong ripple artifacts [21]. We have shown that a small number of transmit plane waves (relative to conventional imaging) is sufficient to significantly reduce the variance of the ripple artifacts in the temperature estimates. Furthermore, this compound imaging technique with both transmit and receive focusing could be achieved in real time. We have also proposed a least-squares fitting method to estimate large elevations in temperature (e.g.,  $T > 50^\circ\text{C}$ ) for which the linear relation between ultrasonic times-of-flight and changes in temperature is no longer valid. Compound imaging with motion compensation and high temperature extrapolation techniques could offer a potentially robust HIFU monitoring technique suitable for real-time *in vivo* applications.

## REFERENCES

- [1] R. Seip, "Feedback for ultrasound thermotherapy," Ph.D. dissertation, EECS, University of Michigan, Ann Arbor, MI, 1996.
- [2] R. Seip and E. Ebbini, "Noninvasive estimation of tissue temperature response to heating fields using diagnostic ultrasound," *IEEE Trans. Biomed. Eng.*, vol. 42, pp. 828–839, 1995.
- [3] A. Gelet, J. Y. Chapelon, R. Bouvier, O. Rouvière, Y. Lasne, D. Lyonnet, and J. M. Dubernard, "Transrectal high-intensity focused ultrasound: Minimally invasive therapy of localized prostate cancer," *J. Endourol.*, vol. 14, pp. 519–528, 2000.
- [4] F. Wu, W. Chen, J. Bai, Z. Zou, Z. Wang, H. Zhu, and Z. Wang, "Pathological changes in human malignant carcinoma treated with high-intensity focused ultrasound," *Ultrasound Med. Biol.*, vol. 27, pp. 1099–1106, 2001.
- [5] H. Cline, K. Hynynen, C. Hardy, R. Watkins, J. Schenck, and F. Jolesz, "MR temperature mapping of focused ultrasound surgery," *Magn. Reson. Med.*, vol. 31, no. 6, pp. 628–636, 1994.
- [6] N. McDannold, L. King, F. Jolesz, and K. Hynynen, "Usefulness of MR imaging-derived thermometry and dosimetry in determining the threshold for tissue damage induced by thermal surgery in rabbits," *Radiology*, vol. 216, pp. 517–523, 2000.
- [7] J. Palussiere, R. Salomir, B. Le Bail, R. Fawaz, B. Quesson, N. Grenier, and C. Moonen, "Feasibility of MR-guided focused ultrasound with real-time temperature mapping and continuous sonication for ablation of VX2 carcinoma in rabbit thigh," *Magn. Reson. Med.*, vol. 49, pp. 89–98, 2003.
- [8] C. Simon, P. VanBaren, and E. Ebbini, "Two-dimensional temperature estimation using diagnostic ultrasound," *IEEE Trans. Ultrason., Ferroelect., Freq. Contr.*, vol. 45, pp. 1088–1099, 1998.
- [9] R. Maas-Moreno, C. Damaniou, and N. Sanghvi, "Tissue temperature estimation in-vivo with pulse-echo," in *Proc. IEEE Ultrason. Symp.*, 1995.
- [10] R. Maas-Moreno and C. Damaniou, "Noninvasive temperature estimation in tissue via ultrasound echo-shifts: Part I. Analytical model," *J. Acoust. Soc. Amer.*, vol. 100, 1996.
- [11] R. Maas-Moreno, C. Damaniou, and N. Sanghvi, "Noninvasive temperature estimation in tissue via ultrasound echo-shifts: Part II. In vitro study," *J. Acoust. Soc. Amer.*, vol. 100, 1996.
- [12] N. Miller, J. Bamber, and P. Meaney, "Fundamental limitations of non-invasive temperature imaging by means of ultrasound echo strain estimation," *Ultrasound Med. Biol.*, vol. 28, no. 10, pp. 1319–1333, 2002.
- [13] C. Le Floch, M. Tanter, and M. Fink, "Self defocusing in Hyperthermia: Experiments and simulations," *Appl. Phys. Lett.*, vol. 74, no. 20, pp. 3062–3064, 1999.
- [14] M. Berson, A. Roncin, and L. Pourcelot, "Compound scanning with an electrically steered beam," *Ultrason. Imag.*, vol. 3, pp. 303–308, 1981.
- [15] S. Jespersen, J. Wilhjelm, and H. Sillesen, "Multi-angle compound imaging," *Ultrason. Imag.*, vol. 20, pp. 81–102, 1998.

- [16] R. Entrekin, P. Jackson, J. R. Jago, and B. A. Porter, "Real time spatial compound imaging in breast ultrasound: Technology and early clinical experience," *Medica Mundi*, vol. 43, pp. 35–43, 1999.
- [17] M. Tanter, J. Bercoff, L. Sandrin, and M. Fink, "Ultrafast compound imaging for 2D motion vector estimation: Application to transient elastography," *IEEE Trans. Ultrason., Ferroelect., Freq. Contr.*, vol. 49, no. 10, pp. 1363–1374, 2002.
- [18] N. R. Miller, K. Bograchev, and J. Bamber, "Ultrasonic temperature imaging for guiding focused ultrasound surgery: Effect of angle between imaging and therapy beams," presented at Brit. Med. Ultrasound Soc. Symp., Harrogate, UK, 2003.
- [19] K. Hynynen, C. Martin, D. Watsmough, and J. Mallard, "Errors in temperature measurement by thermocouple probes during ultrasound induced hyperthermia," *Br. J. Radiol.*, vol. 56, pp. 969–970, 1983.
- [20] E. Ebbini, R. Seip, and P. VanBaren, "Noninvasive temperature measurement for feedback control of thermal therapy using ultrasound phased arrays," presented at Int. Congr. Hypertherm. Oncol. (ICHO), 1996.
- [21] C. Simon, P. VanBaren, and E. Ebbini, "Motion compensation algorithm for noninvasive two-dimensional temperature estimation using diagnostic pulse-echo ultrasound," *Proc. SPIE*, vol. 3249, pp. 182–192, 1998.



**Mathieu Pernot** was born in November 1977 in St. Jean de Maurienne, France. He received an engineer degree in Physics from Ecole Supérieure de Physique et de Chimie Industrielles de Paris (ESPCI) in 2001. In 1999, he worked at Doshisha University in Kyoto (Japan) on nonlinear acoustic propagation in waveguide. He received his M.S. degree in acoustics from University Paris VII in 2001. He is currently a Ph.D. student at Laboratoire Ondes et Acoustique in Paris. His research interests include medical ultrasonic imaging and ultrasonic therapy.



**Mickaël Tanter** was born in December 1970 in Paimpol, France. He received the engineer degree in Electronics of SUPELEC in 1994. In 1999, he received the Ph.D. degree in physics (Acoustics) from the University of Paris VII for his work on the application of time reversal to ultrasonic brain hyperthermia. He is now a researcher in the National French Center of Science (C.N.R.S.) and in 2000 joined the laboratory Ondes et Acoustique at the Ecole Supérieure de Physique et de Chimie Industrielle de la ville de Paris (ESPCI). His current

research interests include wave focusing techniques in heterogeneous media, medical ultrasonic imaging, ultrasonic brain imaging, shear wave propagation in soft tissues for cancer detection, ultrasonic therapy, nonlinear acoustics, active noise control.



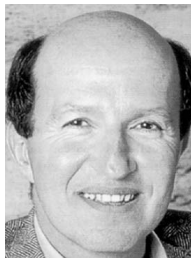
**Jérémy Bercoff** was born in August 1977 in Paris, France. He received, in 2001, the engineer degree from the Ecole Supérieure de Physique et de Chimie de Paris (ESPCI) with a specialization in Physics. In 1999, he worked at ATL Ultrasound, a Philips Medical System company based in Seattle, on the development of echographic systems. In 2000, he received his master's degree at the Laboratoire Ondes et Acoustique in Paris. He is now pursuing his Ph.D. at the Laboratoire Ondes et Acoustique, working on shear wave propagation in soft tissues for cancer detection, ultrafast imaging and flow measurements.



**Kendall R. Waters** (S'92–M'01) was born in 1970 in Chicopee, MA. He graduated from the University of Texas at Austin in 1993 with a B.S. in physics and a B.A. in mathematics. He received his M.S. and Ph.D. degrees in physics (ultrasonics) from Washington University in St. Louis, MO, in 1995 and 2000, respectively.

He worked as a postdoctoral researcher in the Laboratoire d'Imagerie Paramétrique and the Laboratoire Ondes et Acoustique in Paris, France. He is currently an NRC Research Associate at the National Institute of Standards and Technology in Boulder, CO. His research interests include biomedical acoustics, physical acoustics, and nondestructive evaluation.

Dr. Waters is an Associate Editor of the IEEE UFFC Society and a member of the Acoustical Society of America.



**Mathias Fink** received the diplôme de Doctorat de 3<sup>ème</sup> cycle in solid state physics in 1970 and the Doctorat ès-Sciences degree in acoustics in 1978 from the University of Paris VII, Paris, France.

From 1981 to 1984, he was a professor of acoustics at Strasbourg University, Strasbourg, France. Since 1984, he has been a professor of physics at the University of Paris VII (Denis Diderot), Paris, France. In 1990, he founded the Laboratoire Ondes et Acoustique at the Ecole Supérieure de Physique et de Chimie Industrielles de la Ville de Paris (ESPCI). In 2002, he was elected to the French Academy of Technology. In 2003, he was elected to the French Academy of Science.

His current research interests include medical ultrasonic imaging, ultrasonic therapy, nondestructive testing, underwater acoustics, active control of sound and vibration, analogies between optics and acoustics, wave coherence in multiple scattering media, and time reversal in physics. He has developed different techniques in speckle reduction, wave focusing in inhomogeneous media, and ultrasonic laser generation. He holds 28 patents, and he has published more than 300 articles.